The current issue and full text archive of this journal is available at
www.emeraldinsight.com/0961-5539.htm

Received 16 May 2007
Revised 30 October 2007
Accepted 29 November 2007

An *hp*-adaptive finite element model for heat transfer within partitioned enclosures

Darrell W. Pepper
University of Nevada Las Vegas, Las Vegas, Nevada, USA, and
Xiuling Wang
Department of Mechanical Engineering, Purdue University Calumet, Hammond, Indiana, USA

Abstract

Purpose – The purpose of this paper is to describe the development and employment of an *hp*-adaptive finite element method (FEM) algorithm for solving heat transfer problems in partitioned enclosures, which has attracted the attention of both experimental and theoretical researchers in recent years.

Design/methodology/approach – In the *hp*-adaptive FEM algorithm presented here, both the element size and the shape function order are dynamically controlled by an a posteriori error estimator based on the L_2 norm; a three-step adaptation strategy is used with a projection algorithm for the flow solver.

Findings – Simulation results are obtained for 2D and 3D natural convection within partitioned enclosures. Results show refined and enriched elements that develop near the partition edges and side walls of the enclosure, as expected. The heat transfer between the heated and cooled side walls is reduced in the presence of a partial partition.

Research limitations/implications – The Rayleigh numbers were set to 10^5 in the 2D case and 10^3 in the 3D case. Efforts are underway to apply the *hp*-adaptive algorithm to partitioned enclosures at much higher Rayleigh numbers, including comparison with available experimental data.

Practical implications – Heat transfer within partitioned enclosures occurs in many engineering situations: heat transfer across thermo pane windows, solar collectors, fire spread and energy transfer in rooms and buildings, cooling of nuclear reactors and heat exchanger design.

Originality/value – The *hp*-adaptive FEM algorithm is one of the best mesh-based algorithms for improving solution quality, whilst maintaining computational efficiency. The method shows considerable promise in solving a wide range of heat transfer problems including fluid flow.

Keywords Algorithms, Finite element analysis, Convection, Heat transfer

Paper type Research paper

Nomenclature

e	= error (difference between exact and approximate values)	m_i	= diagonal element in lumped mass matrix
h_e	= characteristic element length	N_i	= shape function
h	= element size	p	= pressure, shape function order
K_e	= streamline component of diffusion tensor	P_r	= Prandtl number
		R_a	= Rayleigh number
N_i	= Galerkin weighting function	R_e	= Reynolds number
L	= characteristic dimension	t	= time

International Journal of Numerical Methods for Heat & Fluid Flow
Vol. 18 No. 7/8, 2008
pp. 1000-1014

0961-5539
DOI 10.1108/09615530810899060

T = temperature
T_c, T_h = reference cold and hot temperature
V = velocity vector
W_i = Petrov-Galerkin weighting function
$\mathbf{x}$ = Coordinate vector (x, y, z)
$\boldsymbol{\alpha}$ = Thermal diffusivity
$\hat{\alpha}$ = Petrov-Galerkin weighting factor
β = thermal expansion coefficient
γ = Petrov-Galerkin stability parameter
μ = dynamic viscosity
ν = kinematic viscosity for fluid
ρ = density
σ^* = continuous value obtained from nodal averaging

Introduction

Natural convection within partitioned enclosures occurs in numerous engineering applications, e.g. heat transfer across thermo pane windows, electronic devices cooling, fire spread and energy transfer in rooms and buildings and heat exchanger design. The subject area has been studied widely from both experimental and numerical perspectives.

Chen *et al.* (1990) conducted experiments for 2D steady natural convection within partially divided rectangular enclosures with and without an opening in the partition plate. They noticed that an unopened partial obstruction would reduce the heat transfer rate by 12-30 percent depending on the Rayleigh number, while the opening had little effect on the velocity and temperature profiles of the bottom fluid layer. Khalifa and Abdullah (1999) conducted experiments in 3D, and concluded that the location of the opening and the aperture height ratio both have significant effects on the heat transfer – only a limited effect of aperture width ratio was noticed. Khalifa and Khudheyer (2001) later investigated the effects of 14 different configurations of partitions on the natural convection heat transfer in enclosures.

In addition to various experimental studies, many others have undertaken numerical investigations. Hanjalic *et al.* (1996) used an algebraic turbulent flux model to obtain results for the mean flow and turbulence field as well as Nusselt numbers in 2D partitioned enclosures at high Rayleigh number (Ra ranges from 10^{10} to 10^{12}) with several combinations of boundary conditions. Yucel and Ozdem (2003) used a control volume method with the SIMPLE algorithm to investigate the effect of Rayleigh numbers, number of partitions and heights of partitions on the fluid structure and fluid flow. It was observed that the mean Nusselt number increases with increasing Rayleigh number and decreases with increasing number of partitions. Fu and Shieh (1998) employed a penalty finite element method (FEM) for natural convection heat transfer in a partially divided enclosure for $Ra = 10^4$ and 10^5, and concluded that the heat transfer coefficients were influenced by the baffle height and location. Acharya and Jetli (1990) chose the control volume method with a SIMPLER algorithm to study buoyancy driven heat transfer in a partially divided square box. They found that thermal stratification between the divider and the cold wall played key roles. At lower Rayleigh numbers, the flow was weak in the stratified region and a tendency for flow separation behind the divider was noted. Most of the numerical simulations discussed in the literature are primarily based on 2D geometries.

In an effort to more accurately simulate heat transfer effects in a partitioned enclosure without requiring the use of excessively large meshes, a numerical algorithm based on an *hp*-adaptive finite element strategy has been developed. In the *hp*-adaptive FEM, both the mesh size and the shape function order are dynamically controlled by an a posterior error estimator based on the L_2 norm. The adaptation procedure follows

a three-step strategy: first, an initial coarse mesh is constructed; second, the *h*-adaptive refinement is applied to generate an intermediate mesh; third, a *p*-adaptive enrichment is applied on the intermediate mesh to obtain the final enriched mesh. A discussion on adaptive mesh generation for fluid flow along with advantages and disadvantages of error indicators is given in Nithiarasu and Zienkiewicz (2000).

Wang and Pepper (2007) demonstrated the application of *hp*-adaptive FEM for solving several heat transfer problems. A 2D partitioned enclosure was one of the application cases examined in their study. In the current work, simulations are conducted for 2D and 3D natural convection within partitioned enclosures for laminar flow conditions in an effort to establish adaptive protocols. For the 2D case, different height to length ratios of the partition are adopted. Rayleigh numbers of 10^5 and 10^3 are achieved in 2D and 3D, respectively. Results are characterized by the development of refined and enriched elements near partition edges and side walls, as expected. The heat transfer between the heated and cooled side walls is also reduced in the presence of a partial partition. Results are compared with data in the literature.

The finite element model

Steady state, incompressible laminar viscous flow is assumed with convective heat transfer. Employing the Boussinesq approximation and utilizing the following dimensionless variables, (non-dimensional terms are labeled with "*"):

$$\mathbf{x}^* = \frac{\mathbf{x}}{\mathrm{L}}, \quad \mathbf{V}^* = \frac{\mathrm{V}}{\alpha/\mathrm{L}}, \quad \mathrm{p}^* = \frac{\mathrm{p}}{\rho\alpha^2/\mathrm{L}^2}, \quad \mathrm{T}^* = \frac{\mathrm{T}-\mathrm{T_c}}{\mathrm{T_h}-\mathrm{T_c}}, \quad \mathrm{t}^* = \frac{\mathrm{t}}{\mathrm{L}^2/\alpha} \tag{1}$$

with the Reynolds number (Re), Rayleigh number (Ra), Prandtl number (Pr) and Peclet number (Pe) defined as:

$$\mathrm{Re} = \frac{\rho VL}{\mu}, \quad Ra = \frac{g\beta(T_\mathrm{h}-T_\mathrm{c})L^3}{\alpha\nu}, \quad \mathrm{Pr} = \frac{\nu}{\alpha}, \quad Pe = Ra\cdot\mathrm{Pr} \tag{2}$$

The non-dimensional forms of the governing equations (dropping the asterisk) can be written as:

Conservation of mass:

$$\nabla\cdot V = 0 \tag{3}$$

Conservation of momentum:

$$\frac{\partial\mathbf{V}}{\partial t} + \mathbf{V}\cdot\nabla\mathbf{V} = -\nabla\mathrm{p} + \mathrm{Pr}\,\nabla^2\mathbf{V} + \mathrm{Pr}\,\mathrm{RaT} \tag{4}$$

Conservation of energy:

$$\frac{\partial\mathrm{T}}{\partial\mathrm{t}} + \mathbf{V}\cdot\nabla\mathrm{T} = \nabla^2\mathrm{T} \tag{5}$$

Bilinear quadrilateral elements are used for 2D computational domains and trilinear hexahedral elements are used for 3D problems. The Galerkin weighted residual method is used.

The variables V, T are replaced using the trial functions:

$$\mathrm{V}(\mathbf{x},\mathrm{t}) = \sum_{\mathrm{i}=1}^{\mathrm{n}} \mathrm{N_i}(\mathbf{x})\mathbf{V}_\mathrm{i}(\mathrm{t}) \tag{6}$$

$$\mathrm{T}(\mathbf{x},\mathrm{t}) = \sum_{\mathrm{i}=1}^{\mathrm{n}} \mathrm{N_i}(\mathbf{x})\mathrm{T}_\mathrm{i}(\mathrm{t}) \tag{7}$$

where $\mathbf{x}$ is the physical domain, t is time, i is the degree of freedom (DOF) index and n is the number of DOFs.

A projection algorithm was chosen for the flow solver. The algorithm is based on the Helmhotz-Hodge Decomposition Theorem and was employed by Ramaswamy *et al.* (1992). The matrix equivalent forms for the FEM integral expressions of equations (3)-(5) are straightforward and can be easily obtained. A projection method based on the Helmholtz-Hodge Decomposition theorem is used for the flow solver. Detailed descriptions of the integral formulations and solution procedure are discussed in Wang and Pepper (2007). A Petrov-Galerkin scheme is used to weight the advection terms in the governing equations. The altered weighting function skews the interpolation function in the upwind direction so that the dispersion and added diffusion introduced by the standard Galerkin formulation are minimized, i.e.:

$$W_i = N_i + \frac{\hat{\alpha} h_\mathrm{e}}{2|V|}[V \cdot \nabla N_i] \tag{8}$$

$$\hat{\alpha} = \coth\frac{\gamma}{2} - \frac{2}{\gamma} \tag{9}$$

where $\hat{\alpha}$ is the Petrov-Galerkin weighting factor, h_e is the characteristic element length and γ is the Petrov-Galerkin stability parameter. γ takes on different values depending on the specific case: for only fluid flow problems, $\gamma = |V|h_e\mathrm{Re}$; for fluid flow with forced convection, $\gamma = |V|h_\mathrm{e}\mathrm{Re}\,\mathrm{Pr}$; for flow with natural convection, $\gamma = |V|h_\mathrm{e}\mathrm{Ra}\,\mathrm{Pr}$.

Mass lumping is used in order to obtain a fully explicit time marching scheme, i.e.:

$$[M]^{-1} = \frac{1}{m_i} \tag{10}$$

where m_i is the diagonal element obtained from the sum of the row matrix values.

Adaptation methodologies

Adaptation rules

There are numerous adaptation rules. They are described in detail in various references (Zienkiewicz and Zhu, 1987; Demkowicz *et al.*, 1989; Nithiarasu and Zienkiewicz, 2000; Demkowicz, 2006). However, there are two very important rules: 1-irregular mesh adaptation rule for *h*-adaptation; and minimum rule for *p*-adaptation.

In *h*-adaptation, the 1-irregular mesh adaptation rule must be followed, which is: an element can be refined only if its neighbors are at the same or higher level (1-irregular mesh) (note that the higher the level, the finer the mesh). By following this rule, multiple constrained nodes (parent nodes themselves are constraint nodes) can be avoided. Vertex nodes that lie in the interior of the big element edge, and the two

mid-edge nodes lying on the small element edges are defined as constrained nodes (Demkowicz, 2006). As an example, 2D *h*-adaptation procedure is shown in Figure 1(a)-(c).

In *p*-adaptation the minimum rule must be followed, which is: the order for an edge common between two elements must never exceed the orders of the neighboring middle nodes. As an example, 2D *p*-adaptation procedure is demonstrated in Figure 2(a)-(c).

The adaptation rules for both *h*- and *p*-adaptation must be followed when combined in *hp*-adaptation. Constraints at the interface of elements supporting edge functions of different order are employed to maintain continuity of the global basis function. The DOF of those constraint nodes may be interpreted by certain linear combinations of directional or mixed derivatives. Detailed discussions about the procedure on how to handle such constraints can be found in Demkowicz *et al.* (1989).

Error estimator and adaptation strategy

The error estimator is important in the adaptation procedure. Owing to a poor error estimator, meshes may be refined and enriched in smooth flow region rather than in fast change flow region. There are many error estimators in the literature (Ainsworth and Oden, 2000; Zienkiewicz and Zhu, 1987; Nithiarasu and Zienkiewicz, 2000; Bänsch *et al.*, 2002; Bartels and Cartsensen, 2002; Cartsensen and Bartels, 2002; Hetu and Pelletier, 1992). The estimator developed by Zienkiewicz and Zhu (1987) is easy to implement and provides reasonable accuracy. An extension of this error estimator is utilized here based on the L_2 norm. For example, the error in velocity can be written as:

$$\|e_V\| = \left(\int_{\Omega} e_V^T e_V \, \mathrm{d}\Omega \right)^{1/2} \tag{11}$$

where $e_{\mathbf{V}} = \mathbf{V} - \mathbf{V}^{\mathrm{hp}}$ (exact value – approximate value obtained from the FEM solution) and superscript T denotes the transpose. All element errors can be defined as:

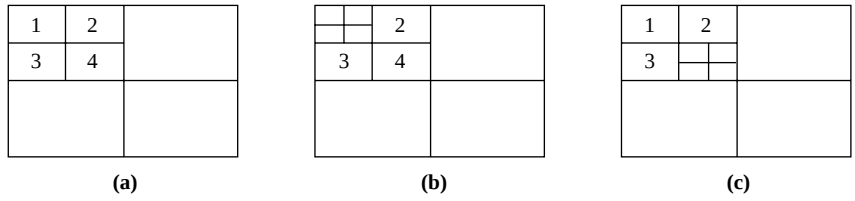

Figure 1.
Examples for *h*-adaptation: (a) initial mesh; (b) correct *h*-adapted mesh; (c) incorrect *h*-adapted mesh

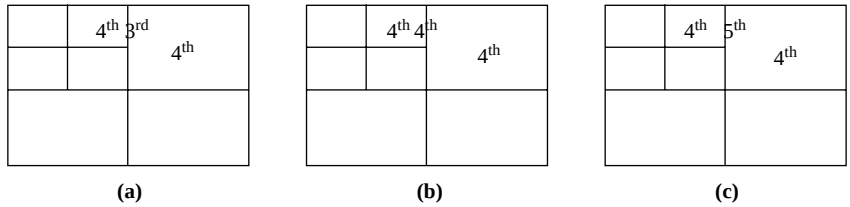

Figure 2.
Examples for *p*-adaptation: (a) initial mesh; (b) correct *p*-adapted mesh; (c) incorrect *p*-adapted mesh

$$\|e_j\|^2 = \sum_{i=1}^{m} \|e_j\|_i^2 \tag{12}$$

where m stands for the total number of elements and j can refer to velocity, pressure, temperature, or stress.

The error index $\eta = \eta_j$, in the form of error percentage, can be defined as:

$$\eta_j = \left(\frac{\|e_j\|^2}{\|\sigma^*\|^2 + \|e_j\|^2} \right)^{1/2} \times 100 \text{ percent} \tag{13}$$

where σ^* stands for exact solutions. Since exact solutions are generally not available, a continuous solution obtained by projection or nodal averaging can be used (Zienkiewicz and Zhu, 1987). In these types of processes, it is assumed that σ^* is interpolated by the same function. The error index η is used to guide the adaptation procedure. Temperature is chosen as the key variable to control the adaptation procedure.

Various adaptation strategies can be found in the literature (several strategies are discussed in Wang and Pepper, 2007). In this study, the *hp*-adaptation procedure is an extension of the "three-step *hp*-adaptive strategy" developed by Oden and Demkowicz (1991) and Oden *et al.* (1995). The error estimator is based on the element residual method-an alternative L_2 norm error estimator (based on temperature). Following the format of equation (11), the estimator for temperature (or temperature gradient) can be defined as:

$$\|e_T\| = \left(\int_\Omega e_T^T e_T \mathrm{d}\Omega \right)^{1/2} \tag{14}$$

An acceptable solution is reached when global and local error conditions are met (Oñate and Bugeda, 1994). A global error condition states that: global percentage error should not be greater than a maximum specified percentage error, $\eta \leq \bar{\eta}_{\max}$. If $\eta > \bar{\eta}_{\max}$, a new iteration is performed. The local error condition states that local relative percentage error of any single element $\|e_T\|_i$ should not be greater than the averaged error $\bar{e}_{avg}$ among all the elements in the domain. For example, the average element error associated with the temperature gradient can be defined as:

$$\bar{e}_{avg} = \bar{\eta}_{\max} \left[\frac{(\|\nabla T^*\|^2 + \|e_T\|^2)}{m} \right]^{1/2} \tag{15}$$

where m is the number of elements in the domain. A local element refinement indicator is defined to decide if a local refinement for an element is needed:

$$\xi_i = \frac{\|e_T\|_i}{\bar{e}_{avg}} \tag{16}$$

when $\xi_i > 1$, the element is refined; when $\xi_i < 1$ the element is unrefined. In an *h*-adaptive process, the new element size is calculated using:

$$h_{new} = \frac{h_{old}}{\xi_i^{1/p}} \tag{17}$$

In a *p*-adaptive process, the new shape function order is calculated by:

$$p_{new} = p_{old}\xi_i^{1/p} \tag{18}$$

A sequence of refinement steps is employed. Three consecutive *hp*-adapted meshes are constructed for solving the system equations in order to reach a preset target error (for all the simulation cases in this study, $e \leq 10^{-6}$): initial coarse mesh, the intermediate *h*-adapted mesh, and the final *hp*-adapted mesh obtained by applying *p*-adaptive enrichments on the intermediate mesh. The *p*-adaptation is undertaken when computational error is close enough to the preset target error.

Numerical examples

The adaptive algorithm is first benchmarked for natural convection in square enclosures without partitions for both 2D and 3D; additional benchmark results are discussed in Wang and Pepper (2007). Results for natural convection within partitioned enclosures are described subsequently for both 2D and 3D.

Natural convection in square enclosure

Two-dimensional natural convection within differentially heated enclosures has been studied for over 40 years (de Vahl Davis and Kettleborough, 1965). Numerical results are usually compared with benchmark data obtained by de Vahl Davis (1983) and others. The enclosure is heated on the left and cooled on the right; the top and bottom walls are insulated ($0 \leq x \leq L, \quad 0 \leq y \leq L$). In this simulation, $Ra = 10^5$ and $Pr = 0.71$.

The final *hp*-adapted mesh is shown in Figure 3. The final mesh consists of 1,372 elements and 6,529 DOFs. The mesh has been automatically refined and enriched within the boundary layers along the walls of the enclosure.

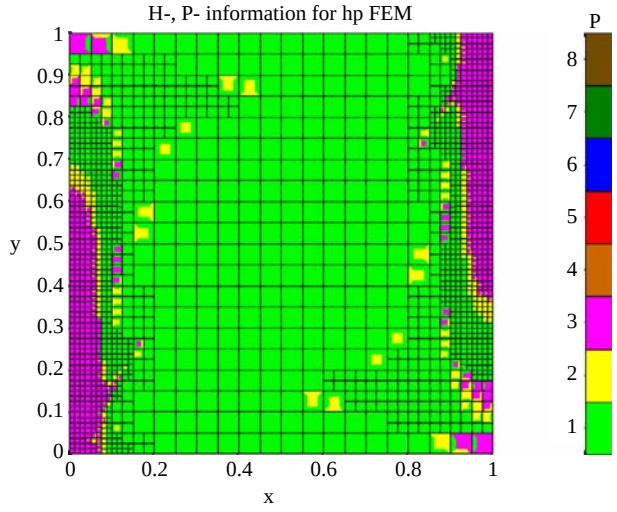

Figure 3.
Final adapted mesh ($Ra = 10^5$)

Steady state results for isotherms and streamfunction contours based on the final mesh are shown in Figure 4(a) and (b). The flow and isothermal patterns compare very well with results from de Vahl Davis (1983).

Quantitative comparisons are shown in Table I for extreme velocities on the horizontal mid-plane together with their locations, and Nusselt numbers along the heated walls with their locations.

Three-dimensional natural convection in a square enclosure is a popular benchmark case – it is an easy extension from 2D. Early solutions for 3D natural convection in an enclosure were typically obtained using the 3D equivalent of the vorticity-stream function form of the equations. One of the earliest simulations was conducted by Mallinson and de Vahl Davis (1977), followed by efforts from many other researchers over several decades (Pepper, 1987; Shaw, 1987; Pepper and Hollands, 2000). For comparison purposes, the cubic enclosure is heated on the right wall and cooled on the left wall. All other walls are insulated ($-0.5L \leq x \leq 0.5L$, $-0.5 \leq y \leq 0.5L$, $-0.5L \leq z \leq 0.5L$) with $Ra = 10^5$ and $Pr = 0.71$.

The initial coarse mesh consisted of 1,000 elements and 1,331 nodes. The intermediate *h*-adapted mesh, shown in Figure 5(a), contained 12,634 elements with 11,718 DOFs. The final *hp*-adapted mesh is shown in Figure 5(b), and consists of 12,634 elements with 29,108 DOFs. As before, the mesh has been automatically refined and enriched within the boundary layers along the walls of the enclosure.

Steady state results for isotherms and velocity vector planes at $y = -0.4$, $y = 0.2$ and $z = 0$ on the final mesh are shown in Figure 6(a) and (b). Flow and isothermal patterns compare well with results found in the literature (Pepper, 1987; Shaw, 1987).

Quantitative comparisons for velocities and Nusselt number are shown in Table II.

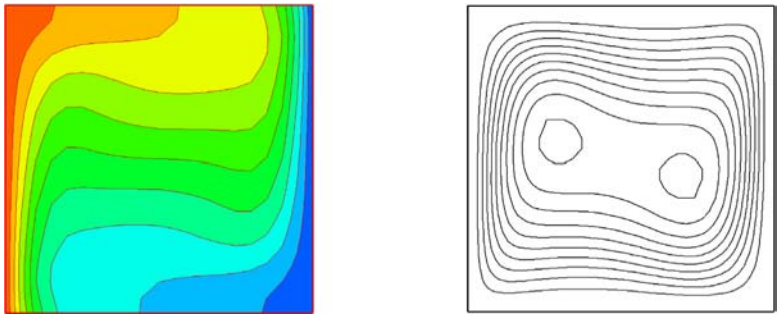

(a) **(b)**

Figure 4.
Simulation results: (a) isotherms (0 to 1 with 0.1 as interval); (b) streamfunctions (−9.509, −8.646 to 0 with 0.9607 as interval) ($Ra = 10^5$)

u_{max} y(x = 0.5)		v_{max} x(y = 0.5)		Nu_{max} y(x = 0)		Nu_{min} y(x = 0)	
(de Vahl Davis)	Present	(de Vahl Davis)	Present	(de Vahl Davis)	Present	(de Vahl Davis)	Present
34.73	34.85	68.59	68.67	7.717	7.720	0.729	0.731
0.855	0.864	0.066	0.070	0.081	0.084	1	1

Table I.
Comparison with benchmark data ($Ra = 10^5$) for 2D natural convection

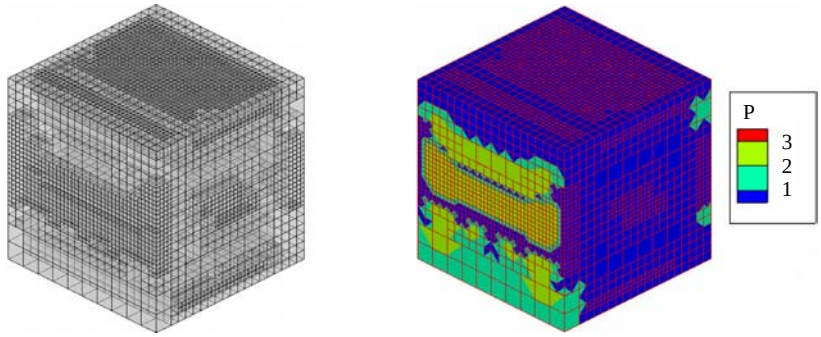

Figure 5.
Adapted meshes: (a) intermediate *h*-adapted mesh; (b) final *hp*-adapted mesh

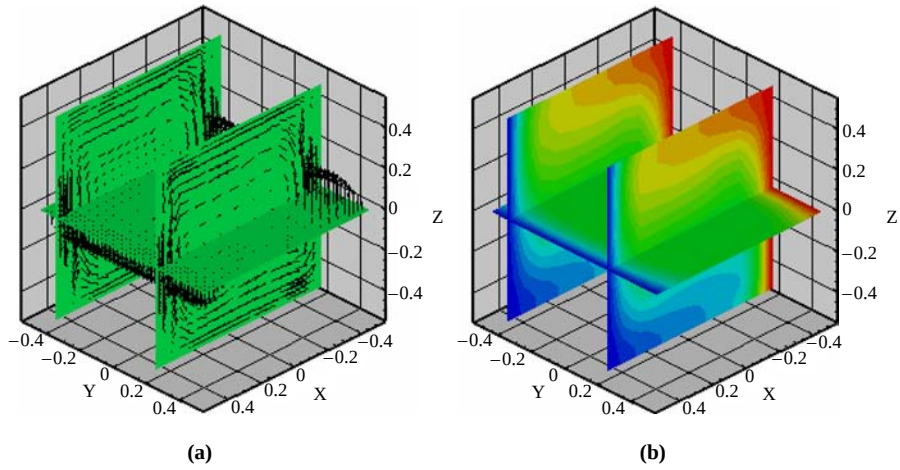

Figure 6.
Simulation results for $y = -0.4$, $y = 0.2$ and $z = 0$ on the final mesh: (a) velocity vectors; (b) isotherms

Table II.
Comparison with benchmark data for 3D natural convection

Case	Ra	u_{max}	v_{max}	Nu_{ave}
3D (Pepper, 1987)	10^5	41.0	69.8	4.62
Present 3D	10^5	40.8	69.2	4.58

Natural convection in partitioned enclosure

Natural convection within a 2D partitioned enclosure is initially presented, followed by a 3D case. A partitioned enclosure has a typical configuration where a partial obstruction extends from a surface, e.g. a printed circuit or a ceiling beam in a room. Such problems have been of interest to the building and HVAC communities for years – recent interest has developed due to homeland security issues associated with partitioned configurations, such as contaminant dispersion within an office complex (Pepper and Wang, 2005). Most published simulation results for natural convection

within a partitioned enclosure have dealt with 2D configurations with few actually encompassing true 3D effects.

For 2D cases, the left and right walls are maintained at hot and cold, respectively; the top and bottom walls, along with the partition surfaces, are insulated. In this simulation, there are two cases with $\mathrm{Ra} = 10^4$ and 10^5 and $\mathrm{Pr} = 0.71$. The computational domain is defined as $0 \leq x \leq L, \quad 0 \leq y \leq L$. The thickness of the partition is 0.1L. The height to length ratio of the partition is $H/L = 0.7$ for case 1 and 0.3 for case 2, the partition is located at 0.7L for both cases. The configuration is shown in Figure 7.

The initial coarse mesh consisted of 372 elements and 427 nodes. The final *hp*-adapted meshes are shown in Figure 8(a) and (b). For $\mathrm{Ra} = 10^4$, the final mesh consisted of 3,102 elements and 8,045 DOFs. For $\mathrm{Ra} = 10^5$, the final mesh consisted of

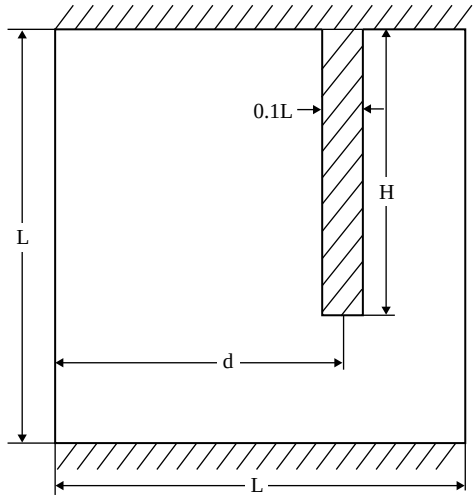

Figure 7.
Problem configuration

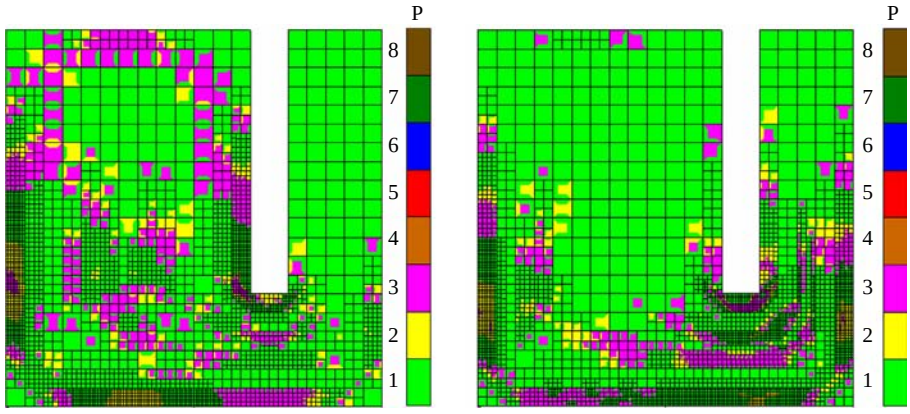

(a) Ra = 10^4 **(b)** Ra = 10^5

Figure 8.
Final adapted meshes

3,558 elements and 8,737 DOFs. Notice that the meshes are refined and enriched along the boundary layers as well as near the partition location. This is due to the acceleration of flow and heat along boundary layers, and can be attributed to regions of high-solution gradient.

Steady state simulation results for isotherms and velocity vectors are shown in Figure 9(a)-(d). Flow and isothermal patterns again compare well with results found in the literature (Fu and Shieh, 1998). As Ra increases, convective effects become more enhanced. The flow begins to intrude into the right upper region, as seen in Figure 9(d), versus less intrusion at lower Ra, as shown in Figure 9(c).

To compare the effects of different partition heights, simulation results for a partition enclosure with height to length ratio of $H/L = 0.3$ are shown in Figure 10 ($\mathrm{Ra} = 10^4$). More details are given in Wang and Pepper (2007). From Figures 9 and 10, it can be seen that the decrease of the partition height enhances the heat transfer from the warm wall to the cold wall, with the flow developing a larger recirculation pattern within the enclosure.

For the 3D case, the top, bottom, front and back walls of the partitioned enclosure are insulated. The left and right walls are maintained at hot and cold temperatures, respectively, with $\mathrm{Ra} = 10^3$. The adiabatic partition baffle (all surfaces of the partition are adiabatic) protruding from the top is 0.1L in thickness and 0.5L in height.

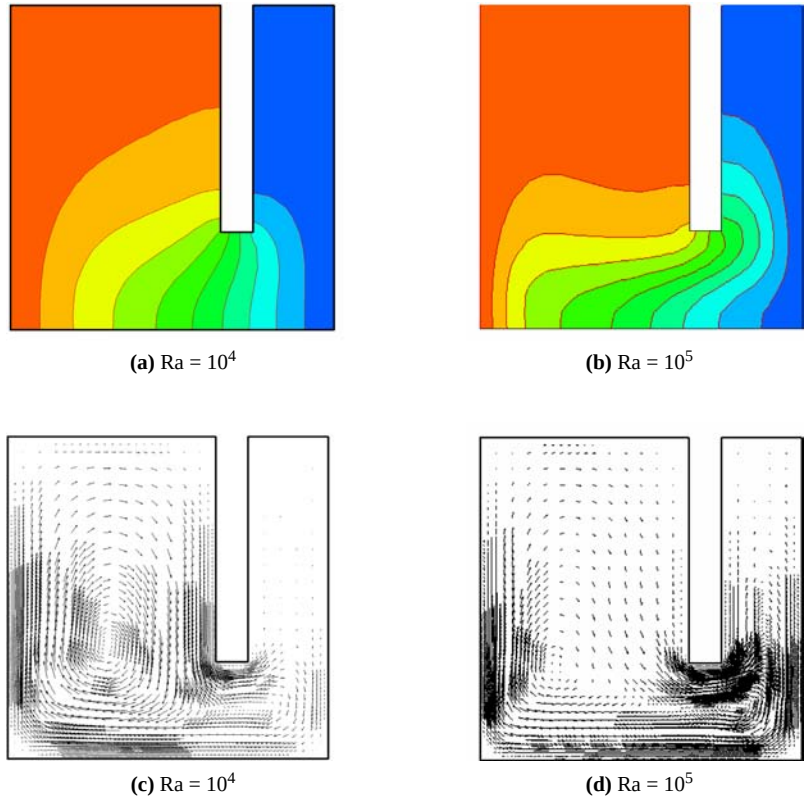

(a) Ra = 10^4

(b) Ra = 10^5

(c) Ra = 10^4

(d) Ra = 10^5

Figure 9.
Simulation results (a) and (b) isotherms, (c) and (d) velocity vectors

The problem domain is defined as $-L \leq x \leq L$, $0 - 0.5L \leq y \leq 0.5L$, $-0.5 \leq z \leq 0.5L$. The configuration is shown in Figure 11.

The intermediate *h*-adapted mesh is shown in Figure 12(a) and consisted of 8,928 elements, 9,668 nodes and 9,668 DOFs. The final *hp*-adapted mesh is shown in Figure 12(b) and contains 8,928 elements, 40,057 nodes and 124,276 DOFs. Notice that the mesh is refined and enriched near the partition corners and in the lower left and right corners due to the acceleration of flow in those regions – and corresponding large errors.

Steady state simulation results for planes at $y = -0.25$, $y = 0.25$ and $z = -0.25$ on the final mesh are shown in Figure 13.

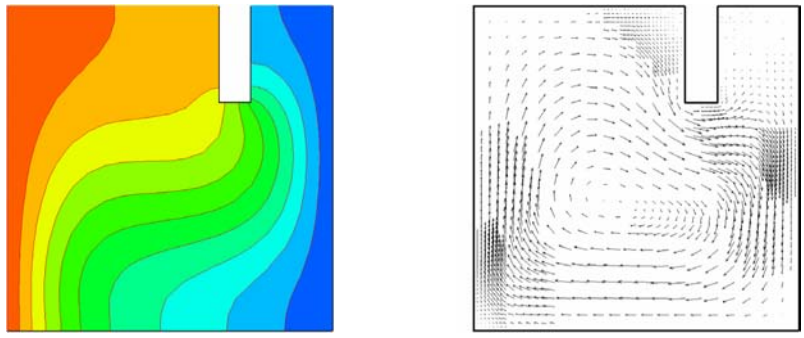

(a) isotherms **(b)** velocity vectors

Figure 10.
Simulation results for $Ra = 10^4$

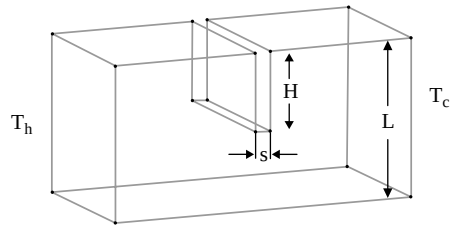

Figure 11.
Partial divided enclosure

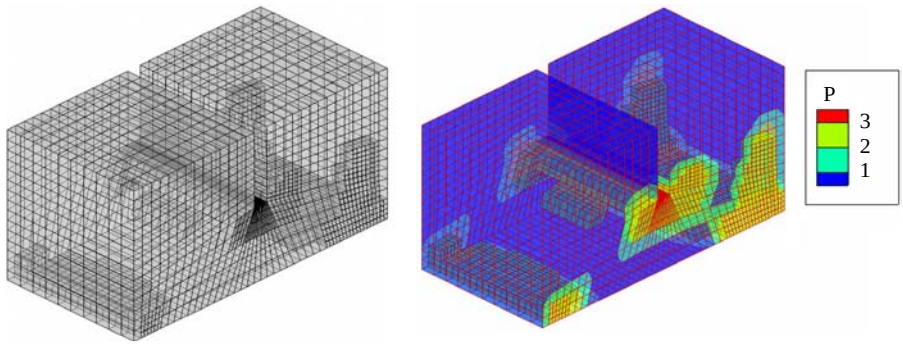

(a) **(b)**

Figure 12.
Adapted meshes: (a) intermediate mesh; (b) final mesh

Flow and isotherm patterns are altered due to the existence of the partition, compared to patterns typically obtained within enclosures without obstructions or partitions. Two recirculation zones can be observed. The flow accelerates beneath the partition with thermal stratification developing along the heated wall side of the enclosure. Such conditions are commonly found in many room configurations, and in thermally stratified lakes where a barrier has been stretched across the lake surface to restrict thermal dispersion (Hamm and Pepper, 1987).

Oden *et al.* (1995) and Nithiarasu and Zienkiewicz (2000) demonstrated the effectiveness of *hp*-adaptivity in computational accuracy and efficiency. More recently Wang and Pepper (2007) show that the employment of *hp*-adaptive FEM algorithms can significantly save computational time versus non-adaptive FEM techniques.

Conclusions

An *hp*-adaptive FEM algorithm is presented for solving the conservation equations of momentum and energy for an incompressible fluid, subjected to differentially heated boundaries. Simulation results are obtained for 2D and 3D natural convection within partitioned enclosures. Results show refined and enriched elements that develop near the partition edges and side walls of the enclosure, as expected. The heat transfer between the heated and cooled side walls is reduced in the presence of a partial partition. The length of the partition projecting from an upper wall also significantly affects the temperature stratification and recirculation pattern within the overall domain. Increased protrusion of the partition into the domain leads to a more localized distribution of temperature near the base of the partition, inhibiting the dispersion of temperature throughout the rest of the domain.

An a posteriori error estimator, based on the L_2 norm, is used to control the adaptation process. The use of the L_2 norm agrees with results from others in showing that the procedure is effective for incompressible flow with heat transfer.

The adaptive FEM produces accurate results at reduced computational cost compared with uniform refined and enriched FEM for the same error criteria. The application of *hp*-adaptive FEM algorithms has been demonstrated repeatedly in the literature to be especially effective for solving a wide range of CFD problems, and should be especially attractive for turbulence simulation. Efforts are under way to solve natural convection problems at higher *Ra* numbers within partitioned enclosures,

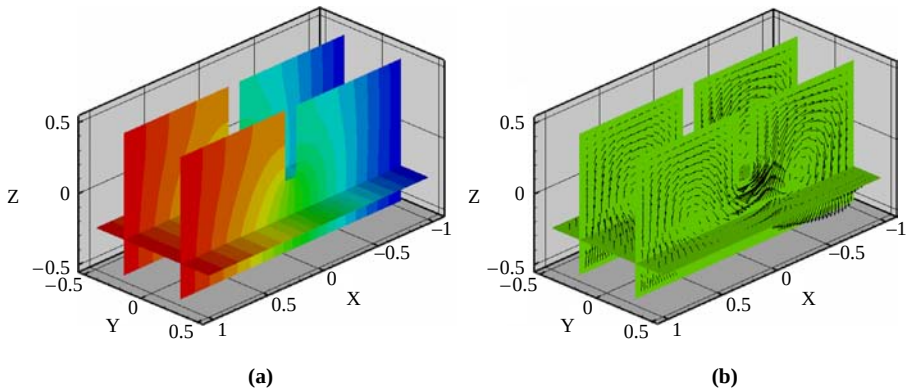

Figure 13.
Simulation results for $y = -0.25$, $y = 0.25$ and $z = -0.25$ on final mesh: (a) isotherms; (b) velocity vectors

including the incorporation of $k - \varepsilon$ and LES closures for turbulent flow. Recent efforts using the *hp* technique have been shown to be particularly effective for modeling indoor ventilation and contaminant transport within building interiors.

References

Acharya, S. and Jetli, R. (1990), "Heat transfer due to buoyancy in a partially divided square box", *International Journal of Heat and Mass Transfer*, Vol. 33, pp. 931-42.

Ainsworth, M. and Oden, J.T. (2000), *A Posteriori Error Estimation in Finite Element Analysis, Pure and Applied Mathematics*, A Wiley-Interscience Series of Texts, Monographs and Tracts, Wiley, New York, NY, p. 264.

Bänsch, E., Morin, P. and Nochetto, R.H. (2002), "An adaptive Uzawa FEM for the Stokes problem: convergence without the inf-sup conditions", *SIAM Journal on Numerical Analysis*, Vol. 40, pp. 1207-29.

Bartels, S. and Cartsensen, C. (2002), "Each averaging technique yields reliable a posteriori error control in FEM on unstructured grids. Part II: high order FEM", *Mathematics of Computations*, Vol. 71, pp. 971-94.

Cartsensen, C. and Bartels, S. (2002), "Each averaging technique yields reliable a posteriori error control in FEM on unstructured grids. Part I: low order conforming, nonconforming and mixed FEM", *Mathematics of Computations*, Vol. 71, pp. 945-69.

Chen, K.S., Ku, A.C. and Chou, C.H. (1990), "Investigation of natural convection in partially divided rectangular enclosures both with and without an opening in the partition plate: measurements", *Journal of Heat Transfer*, Vol. 112, pp. 648-52.

Demkowicz, L. (2006), *Computing with hp-Adaptive Finite Elements, Volume 1: One and Two Dimensional Elliptic and Maxwell Problems*, CRC Press, Boca Raton, FL, p. 398.

Demkowicz, L., Oden, J.T., Rachowicz, W. and Hardy, O. (1989), "Toward a universal hp-adaptive finite element strategy, Part 1. Constrained approximation and data structures", *Computer Methods in Applied Mechanics and Engineering*, Vol. 77, pp. 79-112.

de Vahl Davis, G. (1983), "Natural convection of air in a square cavity: a bench mark numerical solution", *International Journal of Numerical Methods in Fluids*, Vol. 3, pp. 249-64.

de Vahl Davis, G. and Kettleborough, C.F. (1965), "Natural convection in enclosed rectangular cavity", *Institution of Engineers, Australia-Mechanical and Chemical Engineering Transactions*, Vol. MC1, pp. 43-9.

Fu, W.S. and Shieh, W.J. (1998), "A penalty finite element method for natural convection heat transfer in a partially divided enclosure", *International Communications of Heat and Mass Transfer*, Vol. 15, pp. 323-32.

Hamm, L.L. and Pepper, D.W. (1987), "Numerical modeling of a nuclear production reactor cooling lake", paper presented at International Symposium on Modeling Environmental Flows, ASME WAM, Boston, MA, December 13-18.

Hanjalic, K., Kenjeres, S. and Durst, F. (1996), "Natural convection in partitioned two-dimensional enclosures at higher Rayleigh numbers", *International Journal of Heat and Mass Transfer*, Vol. 39, pp. 1407-27.

Hetu, J-F. and Pelletier, D.H. (1992), "Fast, adaptive finite element scheme for viscous incompressible flows", *AIAA Journal*, Vol. 30, pp. 2677-82.

Khalifa, A.J.N. and Abdullah, S.E. (1999), "Buoyancy driven convection in undivided and partially divided enclosures", *Energy Conversion and Management*, Vol. 40, pp. 717-27.

Khalifa, A.J.N. and Khudheyer, A.F. (2001), "Natural convection in partitioned enclosures: experimental study on 14 different configurations", *Energy Conversion and Management*, Vol. 42, pp. 653-61.

Mallinson, G.D. and de Vahl Davis, G. (1977), "Three-dimensional natural convection in a box: a numerical study", *Journal of Fluid Mechanics*, Vol. 83, pp. 1-31.

Nithiarasu, P. and Zienkiewicz, O.C. (2000), "Adaptive mesh generation for fluid mechanics problems", *International Journal for Numerical Methods in Engineering*, Vol. 47, pp. 629-62.

Oden, J.T. and Demkowicz, L. (1991), "Adaptive finite element methods in computational fluid dynamics", *Computer Methods in Applied Mechanics and Engineering*, Vol. 89, pp. 11-40.

Oden, J.T., Wu, W.H. and Ainsworth, M. (1995), "Three-step h-p adaptive strategy for the incompressible Navier-Stokes equations", *The IMA Volume, Modeling, Mesh Generation, and Adaptive Numerical Methods for Partial Differential Equations*, Springer, pp. 347-66.

Oñate, E. and Bugeda, G. (1994), "Mesh optimality criteria for adaptive finite element computations", in Whiteman, J.R. (Ed.), *The Mathematics of Finite Elements and Applications*, Wiley, Chichester, pp. 121-35.

Pepper, D.W. (1987), "Modeling of three-dimensional natural convection with a time-split finite-element technique", *Numerical Heat Transfer*, Vol. 11 No. 1, pp. 31-55.

Pepper, D.W. and Hollands, K.G.T. (2000), "Summary of benchmark numerical studies for 3-D natural convection natural convection in an air-filled enclosure", *Numer. Heat Transfer, Part A*, Vol. 37, pp. 249-70.

Pepper, D.W. and Wang, X. (2005), "A hybrid numerical model for quickly assessing indoor contaminant transport", *WIT Transactions on the Built Environment*, Vol. 82, pp. 53-62.

Ramaswamy, B., Jie, T.C. and Akin, J.E. (1992), "Semi-implicit and explicit finite element schemes for coupled fluid/thermal problems", *International Journal for Numerical Methods in Engineering*, Vol. 34, pp. 675-96.

Shaw, H. (1987), "Laminar mixed convection heat transfer in three-dimensional horizontal channel with a heated bottom", *Numerical Heat Transfer, Part A*, Vol. 23, pp. 445-61.

Wang, X. and Pepper, D.W. (2007), "Application of an hp-adaptive FEM for solving thermal flow problems", *Journal of Thermophysics and Heat Transfer*, Vol. 21, pp. 190-8.

Yucel, N. and Ozdem, A.H. (2003), "Natural convection in partially divided square enclosures", *Heat and Mass Transfer*, Vol. 40, pp. 167-75.

Zienkiewicz, O.C. and Zhu, R.J.Z. (1987), "A simple error estimator and adaptive procedure for practical engineering analysis", *International Journal for Numerical Methods in Engineering*, Vol. 24, pp. 337-57.

Corresponding author
Darrell W. Pepper can be contacted at: dwpepper@nscee.edu